Simulation study of granular compaction dynamics under vertical tapping

D. Arsenović,[1] S. B. Vrhovac,[1,*] Z. M. Jakšić,[1] Lj. Budinski-Petković,[2] and A. Belić[1]
[1]*Institute of Physics, P.O. Box 68, Zemun 11080, Belgrade, Serbia*
[2]*Faculty of Engineering, Trg D. Obradovića 6, Novi Sad 21000, Serbia*
(Received 20 June 2006; revised manuscript received 9 September 2006; published 8 December 2006)

We study, by numerical simulation, the compaction dynamics of frictional hard disks in two dimensions, subjected to vertical shaking. Shaking is modeled by a series of vertical expansion of the disk packing, followed by dynamical recompression of the assembly under the action of gravity. The second phase of the shake cycle is based on an efficient event-driven molecular-dynamics algorithm. We analyze the compaction dynamics for various values of friction coefficient and coefficient of normal restitution. We find that the time evolution of the density is described by $\rho(t)=\rho_\infty-\Delta\rho E_\alpha[-(t/\tau)^\alpha]$, where E_α denotes the Mittag-Leffler function of order $0<\alpha<1$. The parameter τ is found to decay with tapping intensity Γ according to a power law $\tau \propto \Gamma^{-\gamma}$, where parameter γ is almost independent on the material properties of grains. Also, an expression for the grain mobility during the compaction process has been obtained. We characterize the local organization of disks in terms of contact connectivity and distribution of the Delaunay "free" volumes. Our analysis at microscopic scale provides evidence that compaction is mainly due to a decrease of the number of the largest pores. An interpretation of the memory effects observed for a discontinuous shift in tapping intensity Γ is provided by the analysis of the time evolution of connectivity numbers and volume distribution of pores.

DOI: 10.1103/PhysRevE.74.061302 PACS number(s): 45.70.Cc, 61.43.Gt, 81.05.Rm

I. INTRODUCTION

The phenomenon of granular compaction involves the increase of the density of granular material subjected to shaking, tapping or, more generally, to some kind of external excitation. The underlying dynamic and structural properties of compaction process are a subject of great interest for physicists in recent years. The first experiments [1] indicated that the density compaction under tapping follows an inverse logarithmic dependence on the tapping number, $\rho(\infty)-\rho(t) \sim 1/\ln(t)$. More recently, Philippe and Bideau [2] and Ribière *et al.* [3] showed that the compaction dynamics is consistent with the stretched exponential law $\rho(\infty)-\rho(t) \sim \exp[-(t/\tau)^\alpha]$. This experiment has been realized in a geometrical configuration that allows only negligible wall effects, unlike the experimental setup of the Chicago group [1]. Other experiments have been carried out in quite different systems. Experimental studies of Lumay and Vandewalle [4] for two-dimensional (2D) granular systems suggested that the slow compaction dynamics is related to the crystallization driven by the diffusion of defects. In the horizontal shaking experiments [5,6] crystalline arrangements are created in the bulk of the packing during compaction, suggesting that the order is not wall induced. The general conclusion is that different shaking procedures and geometrical constraints give rise to intrinsically different compaction behaviors, driven by different dynamical mechanisms.

A number of different approaches have been proposed in order to connect a very slow compaction of granular materials with role of geometrical frustration. This frustration arises from the excluded volume of the grains, imposing restrictions on their relative positions. Most of the studies have been performed for (off-lattice) adsorption-desorption or parking-lot model [7–9], frustrated lattice gas models [10–13], and one-dimensional lattice models with short-range dynamical constraints [14–17]. Although in all these different cases many glasslike features of real granular materials are reproduced, an explicit connection between the above models and a real granular medium is however still rather tenuous.

A main difficulty in studying compaction is that tapping experiments involve two different series of elementary processes of quite different nature, and realistic models for both of these processes are needed. In the first process, mechanical energy is supplied to a powder in the form of external excitation, and free volume is introduced instantaneously throughout the system. Excitations are followed by the periods of release during which the grains and voids have some freedom to rearrange their positions relative to their neighbors. The waiting time between successive taps is large enough to allow the system to relax, so that the initial state for each tap is the final state from the previous relaxation. The consecutive repetition of both processes, tapping and free evolution, reduces the porosity of the material and makes it denser.

Up to now, there has been no realistic numerical model of the above-described shake cycle. The modeling of both processes, tapping and free evolution, is a rather difficult task, although some procedures have been proposed. Our numerical simulation is based on the ideas of Barker and Mehta [18,19] and Philippe and Bideau [20], with modifications aiming at more realistic treatment of gravitational redeposition of granular particles. The previous models [18–20] may have limited application because of not taking into account the friction and other interparticle forces. However, it is known that some aspects of granular dynamics are strongly dependent on friction, such as granular patterns formation [21] and friction-induced hysteresis [22]. In order to get a physical insight into the mechanisms responsible for the be-

*Electronic address: vrhovac@phy.bg.ac.yu; URL: http://www.phy.bg.ac.yu/~vrhovac/

havior of the system under tapping, the introduction of the material properties for the grains is needed.

Our simulations have been performed for a two-dimensional system of frictional mono-sized hard disks in the rectangular geometry. During the redeposition of the packing, the disks undergo instantaneous, inelastic binary collisions and propagate under gravity in-between collision events. Their settlement is terminated when the total kinetic energy of each disk falls below some threshold value. Previously observed multiparticle structures (arches or bridges) [19,23] are seen to naturally emerge in the simulation. The algorithm employed in the present paper describes, relatively accurately, the quite complex succession of collisions in a shaken packing and provides realistic information about its microstructural transformations during compaction. Completely realistic simulations using, e.g., soft particle methods [24], allowing the determination of forces and interparticle contacts, require much more computational power when applied to dense granular systems.

The plan of the paper is as follows. The simulation methodology is presented in Sec. 2. The results are presented in Sec. III, which is divided into three parts. The first part contains the description of the behavior of global quantities, such as the packing fraction, followed by a discussion about the grain mobility. In the second part, we present the numerical results at the microscopic scale. The third part is devoted to the analysis of the short-term memory effects by considering the response of system to sudden change in the vibration intensity. Finally, the Sec. IV contains concluding remarks and comments.

II. SIMULATION METHOD

In the simulation, the compaction of $N=1000$ monosize disks of diameter d and mass m under consecutive taps is studied in a rectangular container of width $L=1$, with a flat bottom at $y=0$ and opened top. A gravitational field $\vec{g}$ acts downwards, i.e., along the negative y direction. One shake cycle of the granular assembly (corresponding to one time step of our simulation) is decomposed in two stages: (i) vertical dilatation of the disk packing, in proportion to the shaking acceleration Γ, and (ii) formation of static granular pack in the presence of gravity. Repeated application of the shaking algorithm builds a sequence of static packings where each new packing is built from its predecessor.

In the first phase of the shake cycle, free volume is introduced uniformly throughout the whole packing. A disk at height y is raised to a new height $y'=(1+\xi)y$. This models the dilation phase of a vibrated granular medium. In that sense, the parameter ξ in our model plays a similar role as Γ in real experiments. The latter is defined as the ratio of the peak acceleration of the tap to the gravitational acceleration [1]. The exact functional relationship between these two quantities is not known, but in a rough approximation dilation ξ is proportional to the square of the experimental control parameter Γ [20,25].

After dilation, we give a random initial velocity to each disk, in such a way that the total momentum is equal to zero. Let $\langle \Delta E_p \rangle$ denote the average increment of the potential energy per disk during the vertical expansion of the disk packing. Initial linear velocities v_x and v_y are drawn from a uniform distribution in the interval $[-2v_T, 2v_T]$, where $v_T = [2\langle \Delta E_p \rangle / m]^{1/2}$. Similarly, the values of initial angular velocities ω_z are chosen randomly from a uniform distribution in the interval $[-2\omega_T, 2\omega_T]$, where $\omega_T = [2\langle \Delta E_p \rangle / I]^{1/2}$ and I is the moment of inertia about the center of disk. This constitutes the initial condition for the second phase of the shake cycle. The choice of the initial velocity distribution function does not play substantial role in our simulation. We have verified that usage of a different (e.g., Gaussian) distributions for initial velocities give quantitatively very similar results, leading to qualitatively same phenomenology.

In the second phase of the shake cycle, the packing is compressed under gravity, using an efficient event-driven molecular-dynamics algorithm [26]. The disks are assumed to be inelastic with rough surfaces subject to Coulomb friction. In the event-driven method, the disks follow an undisturbed motion, under the influence of gravity, until an event occurs. An event is either the collision of two disks or the collision of one disk with the wall. The trajectories between collision events are parabolic arcs due to the presence of the gravitational field. In order to proceed from one collision to the next, a search of all upcoming collisions, and the time required for collisions to occur, is made. Once the collision pair with the shortest time to the next collision is identified, the system is advanced by that amount of time and the collision is resolved according to collision rules. Particle collisions are modeled using the Walton model [27,28]. This model implies that two disks at contact either slide, following Coulomb's law, or stick together. The collision rule (given in detail in the Sec. II A) takes into account a reduction of normal relative velocity of the two particles and a reduction of total tangential relative velocity. The collisions with the wall are treated in the same way as collisions between particles, except the wall has infinite mass. Using the velocities just before contact, we compute the disks velocities after the contact following Eq. (3). To prevent an inelastic collapse [29–31], we use a coefficient of restitution, which depends on the relative colliding velocity of the particles [Eq. (5)].

With such an algorithm, in which inelastic collapse does not occur, motion of disks will persist indefinitely. However, this sequence of binary collisions with geometrically decreasing space and time scales brings the system to the state where neighboring disks are very close to contact. Solidification occurs because the disks lose almost all of their kinetic energy and move around a fixed positions in similar way as molecules in a crystal. Hence, in the absence of energy input, granular material becomes denser, i.e., system locally "solidifies" due to the dissipation. The local densification is accompanied by the formation of complex patterns and structures in all parts of the system [32].

Because of dissipative collisions, the potential energy of the system tends toward a constant, while its kinetic energy tends toward zero in the long time limit. A static configuration of disks with zero kinetic energy is reached by imposing the following stopping criteria. A disk is considered to be at rest if both translational and rotational kinetic energy of the

disk in the last ten collisions falls below a threshold value $E_{tr}^{(t)}$ and $E_{tr}^{(r)}$, respectively. Here, $E_{tr}^{(t)}$ and $E_{tr}^{(r)}$ are free parameters that are chosen to optimize the computational method. We have verified that for sufficiently small values of $E_{tr}^{(t)}$ and $E_{tr}^{(r)}$ our results are not strongly dependent on this choice. In this study, we used very small values $E_{tr}^{(t)}=5\times10^{-5}$ and $E_{tr}^{(r)}=10^{-6}$, in dimensionless units described in Sec. III.

In order to accelerate the settlement of the packing during the second phase of shake cycle, we introduce an additional algorithm to handle the behavior of a disk bouncing repeatedly off a surface of an immovable disk. Consider a disk that suffers successive inelastic collisions with another disk that is already at rest. During each bounce, a part of the kinetic energy of the disk is dissipated. The normal component of disk velocity after a collision is therefore smaller than before the collision, and consequently, the height of bounces decreases with time. In our case, the coefficient of normal restitution $\varepsilon\rightarrow1$ when the relative velocity of colliding particles is sufficiently low; therefore, the collapse process is never completed. Hence, due to very large bouncing frequency the progression of the event-driven algorithm is suspended. Furthermore, if a disk bounces on the surface of an immovable disk while rolling downward, then its kinetic energy increases due to gravity so that stopping criteria could not be reached.

To circumvent these problems, we use a simple algorithm to detach one bouncing disk from the surface of the immovable disk. The "detachment" procedure includes those disks that have already performed more than ten consecutive collisions with one immovable disk. Consider the disk i, which is bouncing on immovable disk j, and denote with $\Delta\tau_i$ the time interval between two consecutive bounces of disk i. In order to increase the time $\Delta\tau_i$ above certain threshold τ_{tr}, we detach it from disk j in such way that (i) its new position is not closer to any other disk then to the disk j, (ii) it is moved at most by $d\sqrt{2}/10$, and (iii) if the displacement has a vertical component, then the linear velocity of disk is reduced to conserve energy. If the new time interval $\Delta\tau_i$ is still smaller than τ_{tr}, its speed is repeatedly reduced by factor of 3 until $\Delta\tau_i$ becomes larger than τ_{tr}. If it is not possible to extend $\Delta\tau_i$ by reduction of speed, then the disk i is stopped. The threshold time τ_{tr} is tuned to the running average of the time intervals between collision events in the given redeposition phase. It should be noted that only a small number of disks ($<1\%$) are stopped by this criterion. The majority of disks are stopped when their kinetic energy becomes sufficiently low. It is shown below that these procedures allow the formation of complex structural components, such as arches or bridges. Finally, the simulation of the second phase of the shake cycle is finished when all of the disks are stopped using one of the aforementioned stopping criteria.

Even though the described detachment procedure involves slight nonconservation of momentum in cases when vertical displacement is necessary, it does not affect the outcome of the simulation since momentum is conserved in the bulk of the granular gas. The nonconservation only takes place at the boundary with immovable disks, which could be regarded as the effective wall felt by the nonsettled part of the system.

The starting configuration is created by inserting the $N=1000$ disks at nonoverlapping positions within a rectangular region of width $L=1$ that extends in y from $y=0$ to $y=0.5L$. This dilute column of particles (with packing fraction $\rho=0.5$, fixing their diameter at $d=0.01784$) is then allowed to settle down under the influence of gravity. This is done by applying the above-described method for the formation of static granular pack. The initial packing is then generated by using one tap cycle ("zero tap") with the required tap intensity. The initial static packing height is typically about $0.35L$. The observed differences in the initial packing fraction of the system depend on the physical properties of the disks. In general, initial packing created with less dissipative disks were denser than those created with more dissipative disks.

These simulations were performed on parallel cluster computer consisting of 100 Intel processors. A typical simulation of entire compaction process used three CPU days on a single processor.

A. Collision rules

We briefly recall the collision rules for two disks of equal diameter d, mass m, and moment of inertia $I=qm(d/2)^2$ (for homogeneous disks, $q=1/2$). The velocity of particle i is denoted by $\vec{v}_i$, and its angular velocity by $\vec{\omega}_i$. In the following, postcollisional quantities are primed. Let $\vec{n}$ be a unit vector pointing from the center of disk 2 to the center of disk 1. The relative velocity of the contact points is $\vec{v}_r=(\vec{v}_1-\vec{v}_2)+\Delta\vec{c}$, where $\Delta\vec{c}=-(d/2)(\vec{\omega}_1+\vec{\omega}_2)\times\vec{n}$. During a collision the normal component of the relative velocity changes according to $\vec{n}\cdot\vec{v}_r'=-\varepsilon\vec{n}\cdot\vec{v}_r$, where $\varepsilon\in[0,1]$ is the coefficient of normal restitution. Energy dissipation due to surface roughness is modeled by $\vec{n}\times\vec{v}_r'=-\beta\vec{n}\times\vec{v}_r$, where $\beta\in[-1,1]$ is the coefficient of tangential restitution. Experimental data [33] suggest that β depends on the angle γ between $\vec{n}$ and $\vec{v}_r$. The impact angle satisfies $\gamma\in(\pi/2,\pi]$, so that $\cos\gamma=\vec{v}_r\cdot\vec{n}/|\vec{v}_r|<0$. Contacts are sliding for impact angles $\gamma\in(\pi/2,\gamma_0]$ and Coulomb's law is approximately valid in this range. For higher values, $\gamma\in(\gamma_0,\pi]$ contacts are sticking, which is governed by a constant coefficient of tangential restitution $\beta_0\in(-1,1]$ ("roughness coefficient"). These findings can be modeled by an impact-angle-dependent coefficient of tangential restitution [28]

$$\beta(\gamma)=\min\left\{\beta_0,-1-\mu\left(1+\frac{1}{q}\right)(1+\varepsilon)\cot\gamma\right\}, \qquad (1)$$

where μ is the Coulomb friction coefficient. The critical angle γ_0 is given by [28]

$$\cot\gamma_0=-\frac{q}{1+q}\frac{1+\beta_0}{1+\varepsilon}\frac{1}{\mu}. \qquad (2)$$

Equation (2) follows from the requirement that $\beta(\gamma)$ is continuous across the transition (at $\gamma=\gamma_0$) between dominance by Coulomb sliding for $\gamma<\gamma_0$, and "sticking" for $\gamma\geqslant\gamma_0$. This collision model and the conservation laws for linear and angular momenta determine the postcollisional velocities

$$\vec{v}_1' = \vec{v}_1 + \frac{1}{m}\Delta\vec{P}, \quad \vec{v}_2' = \vec{v}_2 - \frac{1}{m}\Delta\vec{P},$$

$$\vec{\omega}_1' = \vec{\omega}_1 - \frac{2}{qmd}\vec{n} \times \Delta\vec{P}, \quad \vec{\omega}_2' = \vec{\omega}_2 - \frac{2}{qmd}\vec{n} \times \Delta\vec{P}, \quad (3)$$

where $\Delta\vec{P}$ is the change of linear momentum of particle 1 and is a function of ε, β_0, and μ:

$$\Delta\vec{P} = -\frac{m}{2}(1+\varepsilon)[\vec{n}\cdot(\vec{v}_1 - \vec{v}_2)]\vec{n} - \frac{m}{2}\frac{q[1+\beta(\gamma)]}{1+q}\vec{n} \times \left[(\vec{v}_1 - \vec{v}_2) \times \vec{n} + \frac{d}{2}(\vec{\omega}_1 + \vec{\omega}_2)\right]. \quad (4)$$

The problem of the inelastic collapse characteristic of the event-driven algorithm [34,35], is handled by using normal restitution coefficient ε dependent on the impact velocity v of the colliding particles [31],

$$\varepsilon(v) = \begin{cases} 1 - (1-\varepsilon_0)\left(\dfrac{v}{v_0}\right)^{1/5}, & v \leqslant v_0, \quad \text{(viscoelastic dissipation)}, \\ \varepsilon_0\left(\dfrac{v}{v_0}\right)^{-1/4}, & v \geqslant v_0, \quad \text{(plastic dissipation)}. \end{cases} \quad (5)$$

The critical impact velocity v_0 separates collisions with viscoelastic and plastic deformations of particles occurring at low and high velocities, respectively. The velocity-dependent restitution coefficient model (5) is frequently used to reduce dissipation in the low-velocity regime (which has also been observed experimentally). Recently, this model has been numerically tested for strongly vibrated granular media [31].

III. RESULTS

In the simulations, we describe the roughness of the surfaces and energy dissipation, using the parameters μ (coefficient of friction) and β_0 (coefficient of maximum tangential restitution), as introduced in Sec. II A. Further mechanisms of energy dissipation are the permanent deformation of a particle during contact and transfer of kinetic energy to thermal energy. We account for these effects using the velocity-dependent coefficient of normal restitution ε.

In order to examine the effects of inelastic and friction properties of grains on compaction dynamics, we used two sets of material parameters. More dissipative and rough disks [referred hereafter as disks (A)] are characterized by coefficients $\varepsilon_0=0.6$ and $\mu=0.4$, whereas with parameters $\varepsilon_0=0.9$ and $\mu=0.2$, we characterize less dissipative disks [disks (B)]. For all of the simulations in this paper, we set $\beta_0=0.5$ [33]. We used the same inelasticity and friction coefficients for grain-grain and grain-wall collisions, including the horizontal base.

All our simulations are run with a fixed diameter of disks $d=0.01784$, and critical impact velocity $v_0=0.02$ [Eq. (5)] in dimensionless units in which the container width L, mass of disks m, and gravitational acceleration g all equal unity. However, in a subsequent presentation of the results on the compaction dynamics, time t is measured in number of taps. The value $v_0=0.02L/\sqrt{L/g}$ ($v_0 \approx 0.06$ m/s for $L=1$ m and $g=9.81$ m/s^2) is chosen, throughout the paper, to represent the typical value for hard metal surfaces [31].

A. Dynamics of compaction

In this section, we present and discuss results regarding temporal evolution of the packing fraction $\rho(t)$. The variation of the packing fraction $\rho(t)$ with the number of shakes t for several tapping intensities ξ is presented in Fig. 1, where more dissipative grains [disks (A)] have been used. The inset of Fig. 1 compares the evolution of normalized packing fraction $\tilde{\rho}(t)=[\rho(t)-\rho(0)]/[\rho(\infty)-\rho(0)]$ for two kinds of grains (A) and (B), for $\xi=3\%$. In order to obtain reasonable statistics, it is necessary to average over many independent runs. Because of the large amount of computation time required to reach steady-state density, the results were averaged over eight simulations for each set of control parameters. The simulation curves are in good qualitative agreement with the experimental data obtained in experiments with a reduced lateral confinement [2,3]. We have observed that compaction dynamics gets slower when tapping intensity ξ decreases. Actually, when a small tapping intensity is applied, the evolution of the density toward steady-state value ρ_∞ takes place on a much wider time scale and, finally, a larger value of the asymptotic packing fraction is achieved.

Recently, we carried out the extensive simulations of reversible random sequential adsorption (RSA) using objects of different sizes and rotational symmetries on a triangular lattice [36]. This lattice-based model can be regarded as a simple model for the compaction of granular objects of various shapes. The model describes the density relaxation of a given slice of the granular material, perpendicular to the tapping force. As a result of a tapping event, particles leave the layer at random. Compaction proceeds when particles fall back into the layer under the influence of gravity. Mapping the model onto the experiment, adsorption event is associated with the annihilation or filling of a void within the packing, whereas a desorption event is associated with the creation of a void. The ratio of desorption to adsorption probability determines the final steady-state density and, within a model, plays a role similar to that of the intensity of

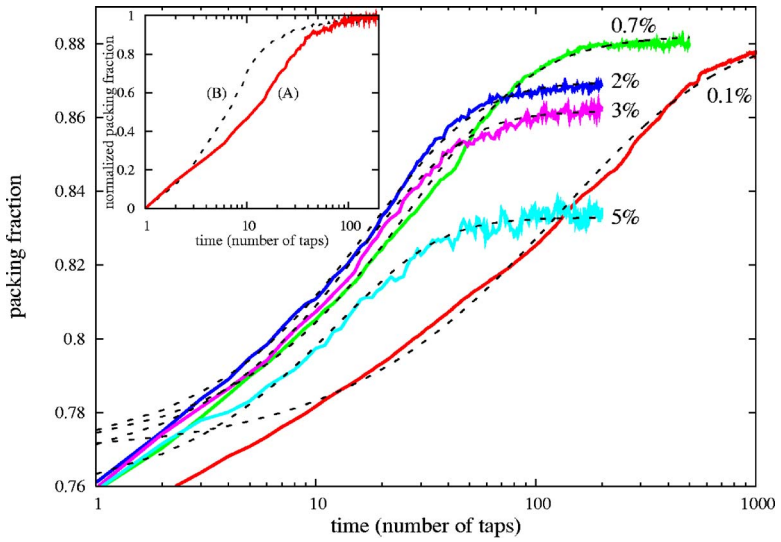

FIG. 1. (Color online) Temporal evolution of the packing fraction $\rho(t)$ obtained for the grains of type (A) and for various tapping intensities ξ =0.1, 0.7, 2, 3, and 5%. The dashed curves are the Mittag-Leffler fits of Eq. (6), with the parameters τ and α given in Fig. 2. Inset: evolution of the normalized packing fraction for two kinds of the grains [disks (A), solid line, and disks (B), dashed line], at ξ=3%.

vibration in real experiments. Note that the dynamics of the reversible RSA model depends on excluded volume and geometrical frustration, just as in the case of granular materials. We showed [36] that the resulting compaction dynamics is strongly consistent with the Mittag-Leffler law

$$\rho(t) = \rho_\infty - \Delta\rho E_\alpha\left[-\left(\frac{t}{\tau}\right)^\alpha\right], \quad \Delta\rho = \rho_\infty - \rho_0, \quad 0 < \alpha < 1. \tag{6}$$

Here, ρ_0 is the initial packing fraction and ρ_∞ is the mean value of the packing fraction at the stationary state. Parameter τ determines characteristic time of the density evolution, and α measures the rate of compaction process on this time scale. E_α denotes the Mittag-Leffler function of order α. It is defined by the following inverse Laplace transform:

$$E_\alpha\left[-\left(\frac{t}{\tau}\right)^\alpha\right] = \mathcal{L}^{-1}\{(u + \tau^{-\alpha}u^{1-\alpha})^{-1}\}, \tag{7}$$

from which the series expansion

$$E_\alpha\left[-\left(\frac{t}{\tau}\right)^\alpha\right] = \sum_{n=0}^{\infty} \frac{[-(t/\tau)^\alpha]^n}{\Gamma(1+\alpha n)} \tag{8}$$

can be deduced. Note that the Mittag-Leffler function is one of the most frequently used phenomenological fitting functions for relaxation processes in many complex disordered systems, such as glasses, ferroelectric crystals, and the dielectrics [37].

Our data are reasonably well fitted by a Mittag-Leffler function (6). These fits are shown by the dashed lines in Fig. 1. Also, some fits of our data are given in Fig. 3. The data we present therein on density $\rho(t)$ are averaged over 80 runs. As can be seen, the intermediate-long-time behavior of the packing fraction can be accurately described by Eq. (6). However, Eq. (6) sometimes fails to reproduce the initial time regime. This can be explained by the short-term memory effects, which will be analyzed in Sec. III C. Indeed, the initial stage of density relaxation depends not only on initial density $\rho(t=0)$ but also on the method used to build an initial packing. Because of that, data fitting has been performed for t after a short transient, typically $t \gtrsim 5-10$ taps.

In Fig. 2, the values of two fitting parameters τ and α vs control parameter ξ are reported for the both kinds of grains, (A) and (B). The parameter τ, for a given type of grain, seems to be a simple power law of the vibration intensity $\xi^{1/2} \propto \Gamma$

$$\tau = K\xi^{-(\gamma/2)}. \tag{9}$$

As one can see from Fig. 2, the slope of the τ vs $\xi^{1/2}$ curves is almost independent on the material properties of the grains. For disks of type (A) and (B), the exponents are $\gamma^{(A)}$=2.50 and $\gamma^{(B)}$=2.85, respectively. However, parameter K of the power law (9) depends appreciably on the material properties of the grains. We have obtained that $K^{(A)}$=30.3 and $K^{(B)}$=13.1 for disks (A) and (B), respectively.

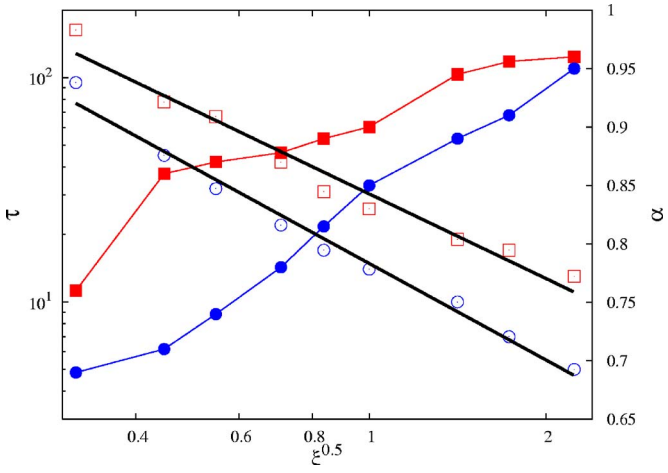

FIG. 2. (Color online) Fit parameters τ (empty symbols) and α (solid symbols) of fit (6), as functions of vibration intensity $\xi^{1/2} \propto \Gamma$ for two kind of the grains. Squares and circles correspond to the grains of type (A) and (B), respectively. The straight lines are fits using Eq. (9). $\tau(\Gamma)$ seems to be well described by simple power law.

This kind of power-law dependence of the parameter τ was also observed in the Mittag-Leffler fits (6) of the coverage fraction in the lattice-based reversible RSA model [36]. We have shown that the parameter τ in this model decreases algebraically with desorption probability P_- as $\tau = K P_-^{-\gamma}$. The exponent γ is the same for all the shapes, $\gamma = 1.29 \pm 0.01$, but the parameter K depends only on the symmetry properties of the shape. The parameter K increases with increasing order of symmetry axis of the shape. This picture supports a physically relevant relationship between lattice-based RSA model and the present model of compaction. In both cases, there is a power-law dependence of parameter τ on the excitation parameters $\xi^{1/2}$ and P_-, which play the same role as the amplitude of the vibration intensity Γ in the real experiments. The exponent γ of this power law can be considered independent of the intrinsic properties of the grains, such as order of symmetry axis of the shape for RSA or dissipative properties of grain for the present model of compaction. Moreover, the shift of the τ vs Γ curves is due to the change of the aforementioned intrinsic properties of the grains.

One striking feature of Fig. 2 is the fact that the fitting parameter α depends considerably on the tapping intensity $\xi^{1/2} \propto \Gamma$ and on the material properties of the grains. For large values of $\xi^{1/2}$, there is a rapid approach to steady-state density ρ_∞ and, consequently, the parameter α reaches a value close to 1. Since $E_\alpha[-(t/\tau)^\alpha] \to \exp(-t/\tau)$ when $\alpha \to 1$, the slow ("glassy") relaxation feature disappears in the regime of strong tapping intensities.

The steady-state density ρ_∞ is also sensitive to material properties of disks. The decrease of ρ_∞ with $\xi^{1/2}$ is more pronounced for disks of type (A). However, for given tapping intensity, the system of disks (B) achieves a larger value of the asymptotic density ρ_∞ than the system of more dissipative disks (A).

It must be emphasized that our simulation curves are compatible with the stretched exponential law [2,3], $\rho(\infty) - \rho(t) \sim \exp[-(t/\tau)^\alpha]$. Similar to Mittag-Leffler law (6), the stretched exponential fit starts to be correct after initial transient time of the order of 5–15 taps, depending on tapping intensity. Both fits give similar correlation coefficients. However, the stretched exponential fit gives somewhat higher values for relaxation times τ.

1. Mobility

The next stage consists of studying the relationship between compaction dynamics and mobility of the grains. The mobility μ is a kinematic property of the system associated with the motion of grains in their nearest-neighbor inside the packing under the action of external gravitation force. Since the gravity is acting along the negative y direction, we concentrate on the drift of the grains that can occur in the vertical direction. In this study, we work with the following definition of the grain mobility:

$$\mu(t) = -\frac{1}{N}\sum_{i=1}^{N} \frac{\langle y_i(t+1) - y_i(t) \rangle}{d}, \tag{10}$$

where N is the number of particles, $y_i(t)$ is the y coordinate of the ith particle at time t, and the angular brackets denote an average over independent runs. Here, time is measured in such a way that unity corresponds to one tap. Hence, μd is equal to the difference in average heights of the center of mass of the system between two consecutive taps.

Earlier studies [38,39] have analyzed the relationship between the mobility of the grains μ and the normalized packing fraction $\tilde{\rho}(t) = [\rho(t) - \rho(0)]/[\rho(\infty) - \rho(0)]$. Recently, Lumay and Vandewalle [4] studied compaction dynamics experimentally for the two-dimensional granular systems. They argued that the Vogel-Fulcher law $\mu \propto \exp[-c/(1-\tilde{\rho})]$ is a good candidate for describing the grain mobilities in dense granular materials. Moreover, they have shown that the evolution of the normalized fraction of the grains belonging to hexagonal domains $\tilde{\phi}$ is well described by the stretched exponential law. Also, they have proposed a new law for compaction dynamics, $\tilde{\rho} = [1 - \exp(-\sqrt{t/\tau})]^{1/2}$, which is compatible with the Avrami model

$$\mu \propto -\frac{1-\tilde{\rho}^2}{\tilde{\rho}\ln(1-\tilde{\rho}^2)}. \tag{11}$$

During compaction, the grains spend most of the time trapped in localized regions or "cages" and occasionally exhibit longer displacements [6,40,41]. As the packing progressively densifies, the time that grains spend in a cage becomes longer and longer and grains move around a fixed position. Thus, when compaction goes on, the grain mobility decreases. We expect that the mobility vanishes when the packing fraction ρ becomes close to its asymptotic or steady-state limit ρ_∞. Hence, the variation of the normalized packing fraction induced by a tap should be proportional to mobility μ,

$$\frac{\partial \tilde{\rho}}{\partial t} = k\mu, \tag{12}$$

where k is a constant.

In a previous work [36], it has been pointed out that the granular compaction dynamics could be described with Mittag-Leffler law (6), which is an alternative to the inverse logarithmic law [1,42] and Kohlrausch-Williams-Watts law [2,3,25]. Substituting Eq. (6) into Eq. (12), we obtain an analytical expression for μ,

$$\mu(t) = -\frac{1}{k}\frac{1}{t}E_{\alpha,0}\left[-\left(\frac{t}{\tau}\right)^\alpha\right]. \tag{13}$$

Here, $E_{\alpha,\beta}$ is generalized Mittag-Leffler function, which possesses the series expansion [43]

$$E_{\alpha,\beta}\left[-\left(\frac{t}{\tau}\right)^\alpha\right] = \sum_{n=0}^{\infty} \frac{[-(t/\tau)^\alpha]^n}{\Gamma(\alpha n + \beta)}. \tag{14}$$

Note that in order to obtain the above expression for mobility [Eq. (13)], we have used the general functional relation for the generalized Mittag-Leffler function [43]

$$\left(\frac{\mathrm{d}}{\mathrm{d}z}\right)^p [z^{\beta-1}E_{\alpha,\beta}(z^\alpha)] = z^{\beta-p-1}E_{\alpha,\beta-p}(z^\alpha), \quad p = 1,2,3,\ldots . \tag{15}$$

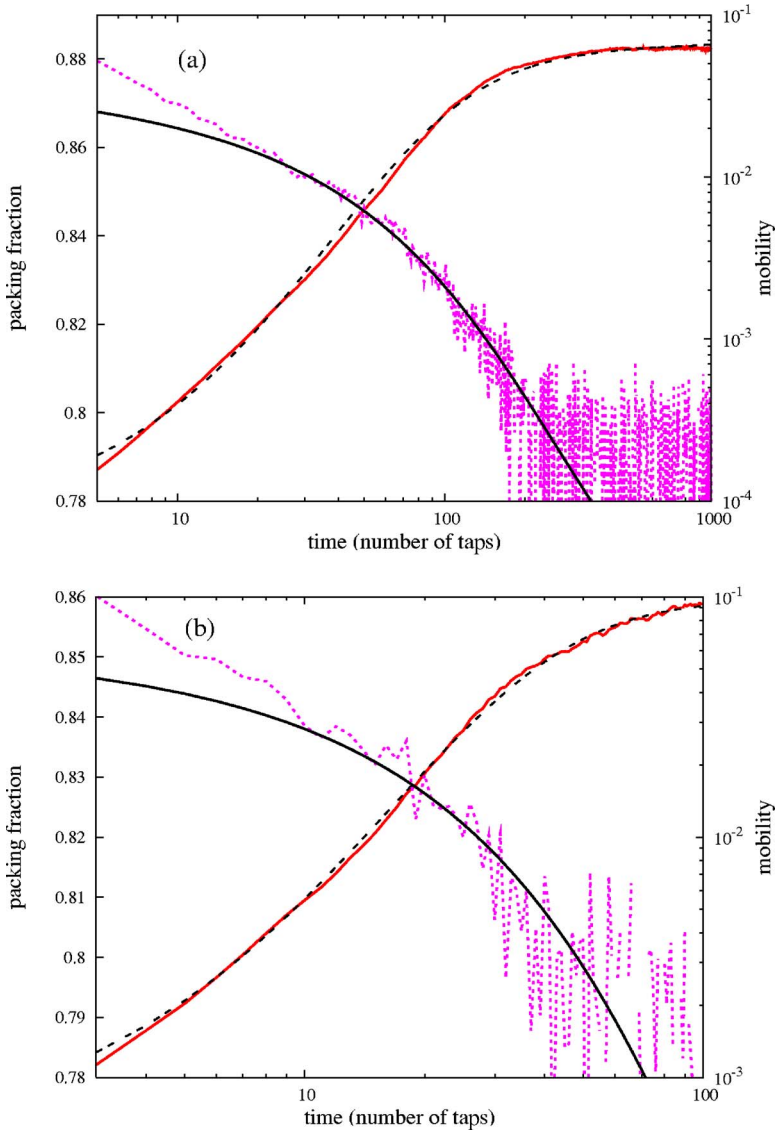

FIG. 3. (Color online) Simulation results for time behavior of the mobility $\mu(t)$ (dotted line) and density $\rho(t)$ (ascending solid line) for two values of the excitation parameter ξ: (a) 0.5% and (b) 3%. These results come from an average over 80 simulations. Parameter k from Eq. (13) is 0.94 and 1.1 for (a) 0.5% and (b) 3%, respectively. The dashed superimposed lines are fits according to Eq. (6). The descending solid curves are mobilities $\mu(t)$ calculated from Eq. (13).

We have checked Eq. (13) by comparing it to the results obtained from the numerical simulation. An example is given in Fig. 3, where we have plotted both mobility $\mu(t)$ and density $\rho(t)$ as functions of the number of taps t. The data shown have been obtained in a system composed of the grains of type (A) and have been averaged over 80 runs. In the same figure the fits to the Mittag-Leffler law Eq. (6) are also given, demonstrating that it is excellently obeyed. The two fitting parameters are $\tau=42.2$, $\alpha=0.878$ for $\xi=0.5\%$, and $\tau=17.1$, $\alpha=0.956$ for $\xi=3.0\%$. The superimposed continuous curves in Fig. 3 are mobilities calculated from Eq. (13) by using the above-quoted fitting parameters. As can be seen, in all cases all the functional forms (13) is quite well satisfied for times beyond initial stage of relaxation process.

A further result can be obtained by relating the mobility μ and normalized packing fraction $\tilde{\rho}$ in the asymptotic limit for large times or densities. For times t large compared to the characteristic time τ, the Mittag-Leffler function decreases algebraically in time

$$E_\alpha\left[-\left(\frac{t}{\tau}\right)^\alpha\right] \sim \frac{1}{\Gamma(1-\alpha)}\left(\frac{t}{\tau}\right)^{-\alpha}, \quad t \gg \tau. \tag{16}$$

From Eqs. (16) and (6), one obtains

$$\tilde{\rho}(t) \sim 1 - \frac{1}{\Gamma(1-\alpha)}\left(\frac{t}{\tau}\right)^{-\alpha}, \quad t \gg \tau. \tag{17}$$

Combining Eqs. (17) and (12), leads to the following relation between μ and $\tilde{\rho}$:

$$\mu = c(1-\tilde{\rho})^{[1+(1/\alpha)]}, \tag{18}$$

where $c=\alpha[\Gamma(1-\alpha)]^{1/\alpha}/(k\tau)$. The power-law scaling (18) describes the mobility μ correctly for sufficiently high values of the normalized packing fraction $\tilde{\rho}$. A similar expression is found for the mobility of highly packed hard-sphere systems [44,45].

It is interesting to note that the fitting function (6) is a solution of the fractional kinetic equation [46]

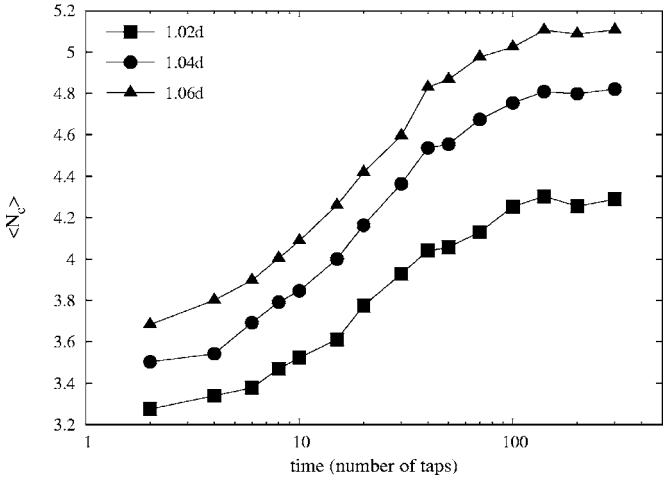

FIG. 4. Evolution of the mean coordination number $\langle N_c \rangle$ during compaction with $\xi=3\%$. Simulation results are given for three values of the cutoff parameter $d_c=1.02d$ (squares), $1.04d$ (circles), and $1.06d$ (triangles).

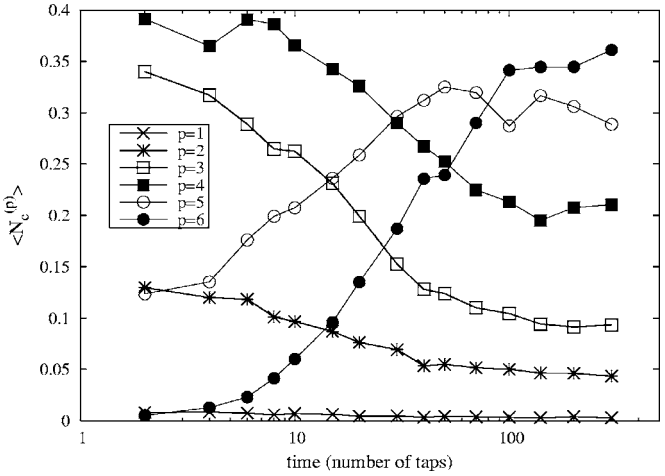

FIG. 5. Simulation results for time behavior of connectivity numbers $\langle N_c^{(p)} \rangle$ for $p=1,\ldots,6$, during compaction with $\xi=3\%$. The cutoff distance d_c is $1.04d$.

$$\frac{\mathrm{d}}{\mathrm{d}t}\Delta\rho(t) = -\tau^{-\alpha}{}_0D_t^{1-\alpha}\Delta\rho(t), \quad 0<\alpha<1, \tag{19}$$

where $\Delta\rho(t)=\rho_\infty-\rho(t)$. Operator ${}_0D_t^{1-\alpha}$ is the Riemann-Liouville (R-L) operator of fractional integration,

$${}_0D_t^{1-\alpha}\Delta\rho(t) = \frac{1}{\Gamma(\alpha-1)}\int_0^t (t-t')^{\alpha-2}\Delta\rho(t')\mathrm{d}t'. \tag{20}$$

The R-L operator introduces a convolution integral into Eq. (19) with the power-law kernel $M(t)\propto t^{\alpha-2}$. Therefore, the fractional kinetic equation (19) involves a slowly decaying memory, so the present density $\rho(t)$ of the system depends strongly on its history $\rho(t')$, $t'<t$. This is in accordance with the fact that granular materials are intrinsically nonlocal.

B. Local analysis

In the previous sections, we reported results on the glassy dynamics of the compaction through the time evolution of both grain mobilities and densities. A further insight into the dynamical mechanisms that take place during compaction can be gained by analyzing the microstructural properties of the packings. In order to analyze the granular organization at the local level, we calculate the number of neighbors for each disk and volume distributions of the pores for packings at different stages of the compaction process.

1. Nearest neighbors

Let us start the analysis of the microstructural properties of the packing configurations by exploring local neighborhoods. The coordination number, i.e., the average number of disks in contact with a given disk is a frequently investigated parameter in the literature on granular packings [47,48]. It varies with the definition of "contact," i.e., the minimal or cutoff distance d_c between two disks below which they are regarded to be in contact. The coordination number is very sensitive to the changes of cutoff distance d_c. Figure 4 shows time evolution of the mean coordination number $\langle N_c \rangle$ during the compaction at three different radial distances: $d_c=1.02d$, $1.04d$, and $1.06d$. The tap intensity was $\xi=3.0\%$, and the results are obtained for the disks of type (A). In all cases, $\langle N_c \rangle$ increases with t and ranges between 3.2 and 5.1, depending on the threshold distance d_c and on the sample density $\rho(t)$. The values of the average number of neighbors at $d_c=1.04d$ for the steady-state packings obtained for various tapping intensities ξ are consistent with the results obtained using both the critical angle model and contact dynamics method [49]. Because of that, in the present work the critical distance was set to $d_c=1.04d$.

Because of dynamic rearrangements in the packing, the number of contact neighbors p varies from particle to particle. In a two-dimensional bed of convex particles, p can vary from 1 to 6. The connectivity of a packing can be characterized by the fraction $\langle N_c^{(p)} \rangle$ of disks having p contact neighbors. $\langle N_c^{(1)} \rangle$ corresponds to "dead ends" of particle chains. $\langle N_c^{(2)} \rangle$ and $\langle N_c^{(3)} \rangle$ are related to chaining and branching, respectively. $\langle N_c^{(4)} \rangle$ corresponds to a situation where a particle is supported by two underlying grains and supports two others ("piling"). $\langle N_c^{(5)} \rangle$ and $\langle N_c^{(6)} \rangle$ correspond to "jammed" and ordered configurations.

Figure 5 shows the variation of the connectivity numbers $\langle N_c^{(p)} \rangle$, $p=1,\ldots,6$ with time (in shaking cycles), as the disks of type (A) are shaken at tapping intensity $\xi=3\%$. All connectivity numbers vary monotonously with time, i.e., with packing fraction. In the whole range of densities, $\langle N_c^{(5)} \rangle$ and $\langle N_c^{(6)} \rangle$ increase at the expense of $\langle N_c^{(2)} \rangle$, $\langle N_c^{(3)} \rangle$, and $\langle N_c^{(4)} \rangle$, which decrease. $\langle N_c^{(1)} \rangle$ remains rather constant during compaction. The initial stage corresponds to the packings characterized by branching and piling (i.e., $\langle N_c^{(3)} \rangle$ and $\langle N_c^{(4)} \rangle$ are the largest connectivity numbers). Relatively large values of $\langle N_c^{(2)} \rangle$ (chaining) suggest the presence of bridges (or arches). The long time regime corresponds to densely ordered packings, where jamming $\langle N_c^{(5)} \rangle$ and ordering $\langle N_c^{(6)} \rangle$ are enhanced. The qualitatively same results are obtained for different val-

ues of the threshold distance in a range between $d_c=1.02d$ and $1.06d$.

One of the most distinctive features in the structure of granular packings is the presence of arches or bridges [19,50,51]. They are responsible for the voids that determine the volume fraction, for the force distributions in granular materials [19], and it has also been proposed as mechanism for the jamming of granular flow in a hopper [52]. An arch or a bridge is a multiparticle structure that is stable, thanks to the contributions of every particle in it. Should any particle of the bridge be removed, the entire bridge would collapse under gravity. It could also be said that a bridge is a set of particles such that we can trace a path of connected particles between any pair in the set [50].

It must be emphasized that our simulations through realistic granular dynamics, together with the stopping criteria, ensures the formation of arches. A great number of particles are involved in such structures. A major mechanism of compaction of weakly vibrated granular materials is the gradual collapse of long-lived bridges, resulting in the disappearance of the voids. In Fig. 6, an evolution of a typical bridge formed in the simulation is shown. The arch is indicated with segments that join mutually stable particles. The chosen images illustrate some characteristic moments of the bridge evolution in the interval between the 48th and 78th tap. The tap intensity was $\xi=0.1\%$, and the images are obtained for the disks of type (A). As it can be seen, during the low-intensity shaking, cooperative structures form and then experience a slow deformation. A bridge, once being formed, usually lasts during a great number of taps. In the high-intensity regime, cooperative structures form and disappear rapidly. Our observation indicates that cooperative structures are preserved for longer times for the lower tap intensities, as expected.

2. Volume distribution of the pores

The volume distribution and shape characteristics of the interstitial voids are important parameters in describing and evaluating the structural properties of granular packings. Volume distribution of the pores can be a test for the free volume theory [38] that postulates an exponential decay for the distribution of these voids, $P(v)\propto\exp(-v/v_0)$, where v is the volume of an individual pore and v_0 is the characteristic size of pores.

The study of how space is repartitioned around the disks is essential for understanding the local arrangement of disks and their local organization. There are several ways to divide the whole space into the parts associated with the local environment around each disk. Voronoi tessellation (VT) [53] is one of the most commonly used partitions. For a given two-dimensional distribution of disks, the VT is a uniquely defined set of convex cells, each of which encloses one and only one of these disks. A Voronoi cell (polygon in two dimensions) associated with a disk is defined as an assembly of points that are closer to that disk than to any of the other disks in the packing. The two disks sharing a common cell edge are neighbors. Each vertex of this tessellation is equidistant to three neighboring disks. As suggested by Philippe and Bideau [20] and Richard *et al.* [54], a pore in 2D pack-

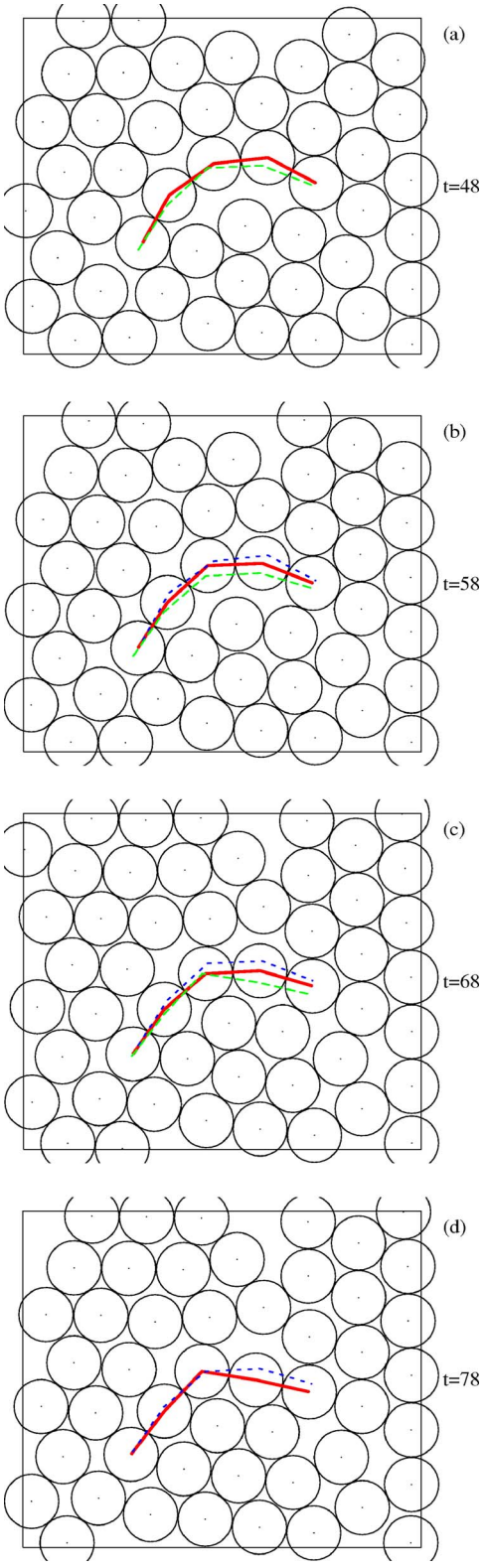

FIG. 6. (Color online) Evolution of bridge (solid line) formed in the simulation with the disks of type (A) and $\xi=0.1\%$. Snapshots display a fragment of the packing after (a) 48, (b) 58, (c) 68, and (d) 78 taps, indicated by thin solid frame. Disks whose centers lie outside of the frame are not shown. The short- and long-dashed lines correspond to bridge position on the previous and the next snapshots, respectively.

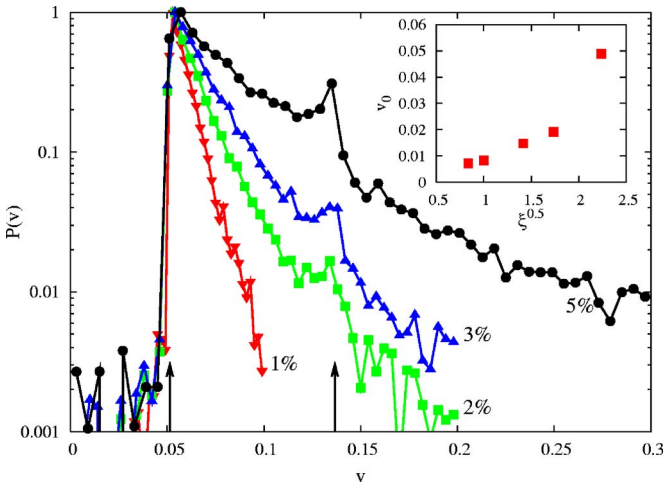

FIG. 7. (Color online) Volume distribution of the pores, normalized by its maximum value, for four different steady-state packings obtained for ξ=1% (down triangles), 2% (squares), 3% (up triangles), and 5% (circles). Vertical arrows are at the volumes $\sqrt{3}/\pi-1/2$ and $2/\pi-1/2$. These results refer to a disks of type (A). Inset: plot of characteristic volume v_0 as a function of $\xi^{1/2} \propto \Gamma$.

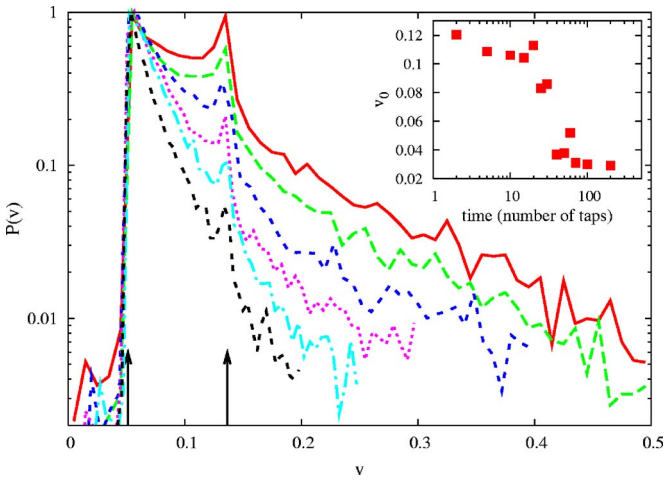

FIG. 8. (Color online) Volume distribution of the pores, normalized by its maximum value, at different stages of compaction. From top to bottom, the lines correspond to t=5, 10, 20, 30, 40, and 100 taps. As t increases, the tail of the distribution corresponding to the largest pores is being reduced. The tapping intensity is ξ=3%. Vertical arrows are positioned as in Fig. 7. These results refer to a disks of type (A). Inset: evolution of the characteristic volume v_0 during compaction.

ing can be defined as a virtual circle centered on the vertex and in contact with the three neighboring disks. The second convenient definition of a pore is based on the Delaunay triangulation (DT), which is a natural way to subdivide a 2D packing structure into a system of triangles with vertices on the centers of neighboring disks. The DT is related to the Voronoi diagram because the circle circumscribed about a Delaunay triangle has its center at the vertex of a Voronoi polygon. In this study, we define the pore as a part of the Delaunay triangle not occupied by the disks (Delaunay "free" volume) [47,55].

First, we compare volume distribution of the pores $P(v)$ for steady states corresponding to different intensities of excitation ξ, as reported in Fig. 7. Here the steady-state pore distributions obtained for ξ=1%, 2%, 3%, and 5% have been plotted; their steady-state packing fractions are, respectively, 0.876, 0.868, 0.863, and 0.832. The pore volume v is normalized by the volume of the grains, $v_d=d^2\pi/4$. It can be seen that these distribution functions are strongly dependent on the intensity of the vibrations. These distributions become narrower when steady-state density increases. Moreover, we observe the appearance of two sharp peaks of $P(v)$ on fixed positions, approximately at 0.05 and 0.14. It is easy to understand which kind of local configuration contributes most to each peak of the $P(v)$. The Delaunay cells with free dimensionless volume $\sqrt{3}/\pi-1/2 \approx 0.0513$ correspond to local arrangements of hexagonal symmetry, when three disks are all in touch with each other with centers on the vertices of a unilateral triangle. The cells with free volume $2/\pi-1/2 \approx 0.1366$ correspond to local configurations of quadratic symmetry, when four disks are all in touch with each other with centers on the vertices of a square. We have verified that other choices for the elementary volumes, such as the void volume proposed by Philippe and Bideau [20] and Richard *et al.* [54], do not yield to such neat second peak in the volume distribution.

Further evidence of transformation in the packing microstructure is provided by the study of evolution of the volume distribution of pores $P(v)$ during compaction. Figure 8 shows the evolution of the $P(v)$ for ξ=3.0% at different stages of the compaction. Here again, the curves of volume distribution $P(v)$ are asymmetric with a quite long tail on the right-hand side, which progressively reduces while the packing structure gets more compact. The tails of such distributions can be fitted by an exponential law, $P(v) \propto \exp(-v/v_0)$. A time evolution of the characteristic volume v_0 is shown in the inset of Fig. 8. It is observed that the coefficient v_0 for steady-state packings depends on the tap intensity $\xi^{1/2} \propto \Gamma$ as shown in the inset of Fig. 7.

It must be noted that very similar behaviors were also found for the distributions of the Delaunay free volumes in the three-dimensional samples of the spheres [47,55]. But, unlike in the two-dimensional case, such configurations do not lead to the appearance of peaks on the exponential tail of volume distribution of the pores. This absence is expected since the tendency toward a crystalline order is much less pronounced in three dimensions than it is in two [4]. Indeed, in two dimensions the densest possible local configuration (hexagonal packing) can be repeated infinitely in space. However, in three dimensions the closest attainable local configuration in a system of equal spheres is not compatible with translational symmetry and therefore it cannot be repeated in space without leaving gaps. After packing 12 spheres around the central one, with centers on the vertices of a regular icosahedron, there is a significant amount of free space left, although not enough to fit 13th sphere. Such a compact local icosahedral configuration is geometrically frustrated, and therefore, it can be regarded as a source of structural heterogeneity.

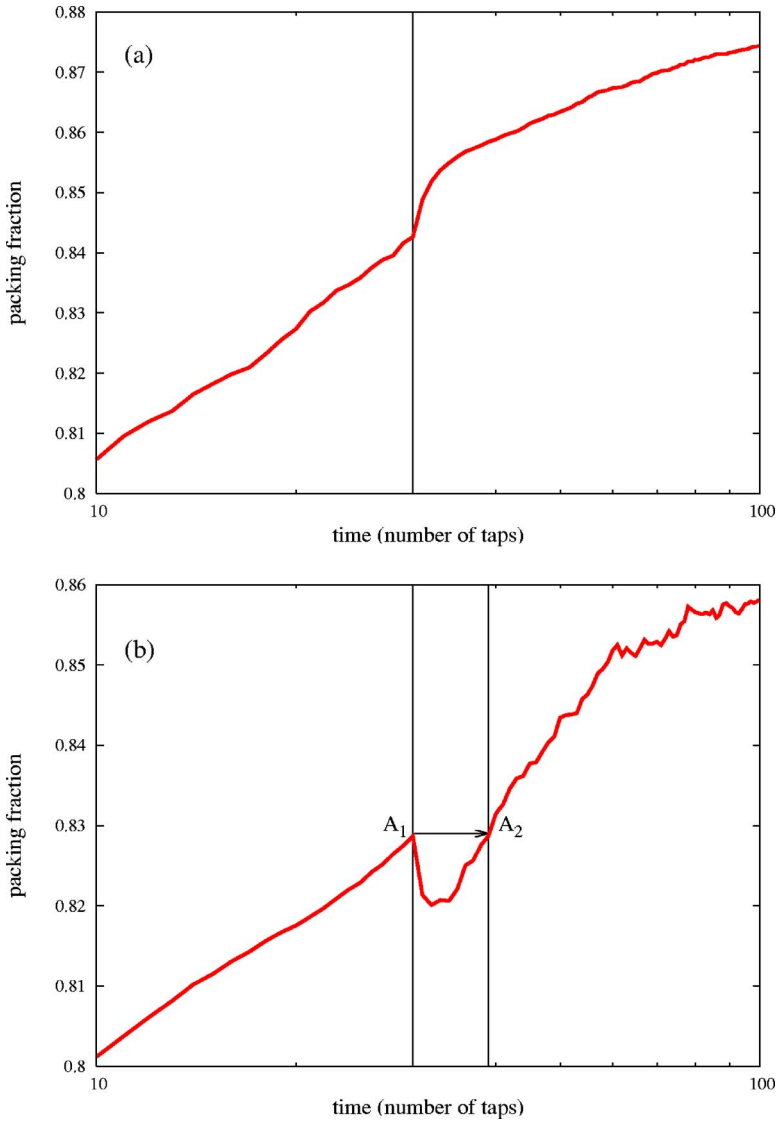

FIG. 9. (Color online) Time evolution of the packing fraction $\rho(t)$ when the tapping intensity ξ is changed at $t_w=30$: (a) from 3 to 0.5%, and (b) from 0.5 to 3%. Points A_1 and A_2 correspond to the packings with equal density $\rho(t_w)=0.828$, at $t_1=30$ and $t_2=39$.

C. Memory effects

In this section, we report how the memory effects are reproduced within our simulation and discuss the accompanying transformations of geometrical structure of disk packings. The nature of the system's relaxation properties can be studied by allowing the tap intensity to "shift" from constant value Γ_1 to another constant value Γ_2 at a given time t_w. Recently, it has been shown [6,56] that, during the compaction, the response to an abrupt change in the amplitude of excitation (the tap intensity Γ or the shear amplitude), is opposite to what could be expected from the long-time behavior of the compaction. For a sudden decrease in Γ, it was observed that on short-time scales the compaction rate increases, while for a sudden increase in Γ the system dilates for short times. This behavior is transient, and after several taps, the usual compaction rate is recovered. Response properties of granular media and the observation of short-term memory effects have motivated a number of numerical or theoretical models based on the free volume concept and geometrical constraints [9–12,15,17,57,58]. The goal of this section is the study the link between the macroscopic dynamics and the microscopic structure of the packing during short-term memory effect.

Figure 9 shows typical memory effects at short times after an abrupt change of tapping intensity ξ. Tapping intensity ξ is switched from 3% to 0.5% and vice versa at $t_w=30$. We observe that after several taps the "anomalous" response ceases and there is a crossover to the "normal" behavior, with the compaction rate becoming the same as in constant forcing mode.

The response in the evolution of the density to a change in the tapping intensity at a given time is accompanied by transformation of the local configurations in the packing. As an example, the evolution of connectivity numbers $\langle N_c^{(p)}\rangle$, $p=1,\ldots,6$ are shown in Fig. 10 for jump ξ:0.5% $\rightarrow$3%, at $t_w=30$. We find that the impact of the sudden increase in the tapping intensity ξ is pronounced for particles having 2, 3, 5, and 6 neighbors. When the tapping intensity ξ is abruptly increased at t_w, the first effect is that the particles tend to decrease the fraction of the packing composed of dense ordered domains. Connectivity numbers $\langle N_c^{(5)}\rangle$ and $\langle N_c^{(6)}\rangle$ decrease rapidly, and the system becomes less compact. Simul-

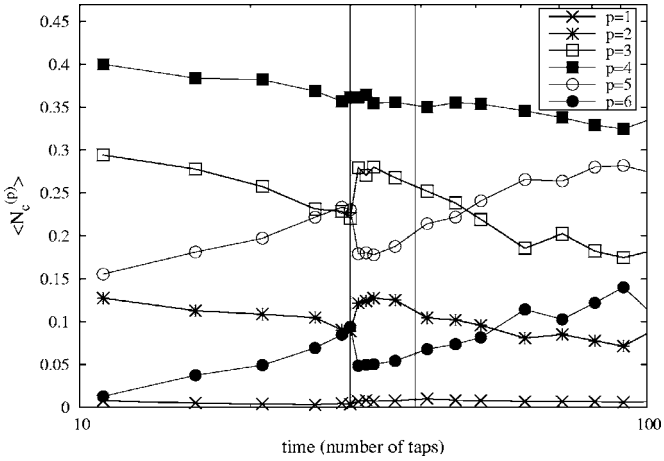

FIG. 10. Time evolution of the connectivity numbers $\langle N_c^{(p)} \rangle$ for $p=1,\ldots,6$, when the tapping intensity ξ is changed at $t_w=30$, from 0.5 to 3%. The thin vertical lines correspond to the states with equal density $\rho(t_w)=0.828$, at $t_1=30$ and $t_2=39$, but different "connectivity disorder." These data refer to a threshold distance $d_c=1.02d$.

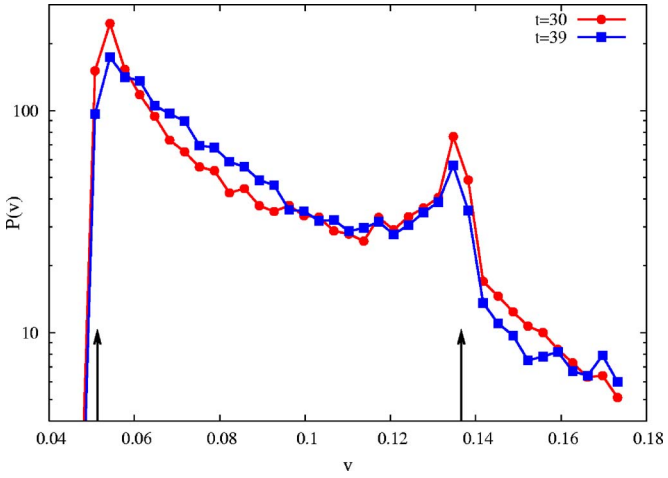

FIG. 11. (Color online) Distributions of Delaunay free volumes for the packings at points A_1 (circles) and A_2 (squares) in Fig. 9. These distributions correspond to packings having the same density. Vertical arrows are positioned as in Fig. 7.

taneously, chaining ($\langle N_c^{(2)} \rangle$) and branching ($\langle N_c^{(3)} \rangle$) increase rapidly. After the transient interval, $\langle N_c^{(5)} \rangle$ and $\langle N_c^{(6)} \rangle$ increase again, at the expense of $\langle N_c^{(2)} \rangle$ and $\langle N_c^{(3)} \rangle$, which decrease.

Memory effect implies that the system can be found in states, characterized by the same packing fraction ρ, that evolve differently under further tapping with the same intensity ξ. This is illustrated in Fig. 9. The points A_1 ($t_1=t_w=30$) and A_2 ($t_2=39$) correspond to states with equal density $\rho(t_w)=0.828$, equal value of $\xi=3\%$, but different further evolution. Their responses to the same tapping intensity $\xi=3\%$ are different: packing A_1 becomes looser, whereas packing A_2 pursues its compaction. In other words, the density evolution after the points A_1 and A_2 depends not only on the density $\rho(t_w)$, but also on the previous tapping history. The memory of the history up to the density $\rho(t_w)$ is encoded in the arrangement of the grains in the packing. As illustrated in Fig. 10, the connectivity of packing is not unambiguously determined by the density $\rho(t_w)$ and tapping intensity ξ. These results suggest that changes in the volume of granular packing are not due to changes in the mean distance between grains. Compaction are driven by the cooperative reorganization of grains as "nodes" of the contact network.

Memory effects reproduced in the present simulation implies that knowing the volume fraction of the packing is not sufficient to predict the evolution of the system. Our results show that the volume distribution of pores $P(v)$ is very sensitive to small structural changes during granular compaction. It qualifies the $P(v)$ as a natural candidate for an additional parameter that unambiguously characterizes the macrostate of the system with fixed ρ and ξ. One can indeed check that the two states A_1 and A_2 described above correspond to distinct values of $P(v)$. Volume distributions of pores in Fig. 11 correspond to packings having the same volume fraction $\rho(t_w)=0.828$. The shapes of distributions $P(v)$ for A_1 ($t_w=30$) and A_2 ($t_1=39$) packings are globally similar, but the differences are perceptible. For volumes $0.06 \lesssim v \lesssim 0.11$, the distribution $P(v)$ for packing A_1 is slightly lower than for packing A_2. However, for the pores larger then ≈ 0.11 and less than ≈ 0.06, we observe an opposite effect on $P(v)$.

IV. FINAL REMARKS

We have demonstrated that numerical simulations of granular compaction offer insight into the dynamics of the compaction process and evolution of the packing structure during its progressive densification. Unlike almost all previous models for granular compaction, whose essential ingredient is geometrical frustration, our model is based on realistic granular dynamics. One of its main features is that during the second phase of the shake cycle the whole system is reassembled by using event-driven molecular-dynamics algorithm. We employed the Walton model [27,28], which captures the major features of granular interactions.

We have fitted the time dependences of the packing fraction with the Mittag-Leffler function (6). Our data show that the compaction dynamics strongly depends on the material properties of the grains. It was shown that the relaxation behavior is appreciably slowing down with the increase of the inelasticity of the grains. The characteristic time scale τ is found to decay with tapping intensity Γ according to a power law (9), $\tau \propto \Gamma^{-\gamma}$. The exponent γ is almost independent on the material properties of the grains.

It is noticeable that such behavior of fitting parameter τ shares some similarities with the compaction dynamics observed in two-dimensional lattice based reversible RSA model [36]. The symmetry properties of the extended objects in RSA model, via this analogy, gets related to dissipative properties of the grains in the present model. Indeed, these intrinsic properties of the grains are responsible in the both models for slowing down of the compaction dynamics. In particular, multiparticle events in reversible RSA model are responsible for the density growth above jamming limit. The increase of the order of symmetry of the shape enhances the rate of single-particle readsorption [36]. This extends the

mean waiting time between two consecutive multiparticle events and causes a slowing down of densification.

In our numerical model, changing the coefficient of normal restitution ε affects the relaxation dynamics during the second phase of shake cycle only by increasing the removal rate of kinetic energy. Therefore, for very dissipative grains, the system might be expected to stop readily in the dilute final state. Thus, the packing fraction in a system of less dissipative grains is the larger than in a system of more dissipative grains prepared by the same number of taps, as more interstitial space is created by more efficient arch building in the latter case.

However, it is not clear whether Eq. (6) is just a convenient fitting expression with four parameters or it has a more fundamental meaning, associated to some peculiar dynamical events that are dominant in the relaxation of the density. We hope to elucidate this point more thoroughly in a future work in order to develop a fractional model of granular compaction that captures this relaxation dynamics.

In order to study the dynamics of compaction, we have also analyzed the mobility of the grains. We have proposed an analytical expression (13) for mobility that is consistent with simulation data.

The organization of grains at the local level was first studied by analyzing the time evolution of connectivity numbers $\langle N_c^{(p)} \rangle$. Observed changes of connectivity numbers have provided additional insight into the formation of cooperative structures during compaction, such as arches or bridges (arching is directly related to the reduction of particle-particle contacts). We have observed that collective rearrangements of the grains in a two-dimensional system lead to growth of hexagonal domains [4].

The reorganization of the grains have also been analyzed through the distribution of the pores volumes. It has been pointed out that this distribution is very sensitive to small structural changes of the system. Delaunay free volumes have a distribution with a long tail, which progressively reduces while the packing gets more compact. In particular, unlike in the three-dimensional case, these distributions have two large peaks that clearly indicate existence of local configurations with hexagonal and quadratic symmetry.

We have also investigated the response of a vibrated granular system to an instantaneous change in the intensity of vibration. Our results are in qualitative agreement with experimental observations [56]. The short time change in the compaction rate has an opposite sign than that of the change of the vibration intensity. The numerical experiments confirm that the global packing fraction alone is not sufficient to describe a static packing, because the future evolution of density depends not only on its current value, but also on the previous tapping history. We have demonstrated that the packings with the same density, but reached with different compaction procedures, have different volume distributions of pores and, consequently, respond in a different way to the same tapping intensity. Qualitatively, this effect reflects the heterogeneity of the system. Indeed, fixing the overall (macroscopic) value of the packing fraction and tapping intensity does not prevent the existence of local fluctuations, which keep track of the system history.

ACKNOWLEDGMENT

This research was supported by the Ministry of Science of the Republic of Serbia, under Grant Nos. 141035 and 141003.

[1] J. B. Knight, C. G. Fandrich, C. N. Lau, H. M. Jaeger, and S. R. Nagel, Phys. Rev. E **51**, 3957 (1995).
[2] P. Philippe and D. Bideau, Europhys. Lett. **60**, 677 (2002).
[3] P. Ribière, P. Richard, D. Bideau, and R. Delannay, Eur. Phys. J. E **16**, 415 (2005).
[4] G. Lumay and N. Vandewalle, Phys. Rev. Lett. **95**, 028002 (2005).
[5] M. Nicolas, P. Duru, and O. Pouliquen, Eur. Phys. J. E **3**, 309 (2000).
[6] O. Pouliquen, M. Belzons, and M. Nicolas, Phys. Rev. Lett. **91**, 014301 (2003).
[7] A. J. Kolan, E. R. Nowak, and A. V. Tkachenko, Phys. Rev. E **59**, 3094 (1999).
[8] J. Talbot, G. Tarjus, and P. Viot, Phys. Rev. E **61**, 5429 (2000).
[9] J. Talbot, G. Tarjus, and P. Viot, Eur. Phys. J. E **5**, 445 (2001).
[10] M. Nicodemi and A. Coniglio, Phys. Rev. Lett. **82**, 916 (1999).
[11] A. Barrat and V. Loreto, J. Phys. A **33**, 4401 (2000).
[12] A. Barrat and V. Loreto, Europhys. Lett. **53**, 297 (2001).
[13] A. Fierro, M. Nicodemi, and A. Coniglio, Phys. Rev. E **66**, 061301 (2002).
[14] J. J. Brey, A. Prados, and B. Sanchez-Rey, Phys. Rev. E **60**, 5685 (1999).
[15] J. J. Brey and A. Prados, Phys. Rev. E **63**, 061301 (2001).
[16] A. Prados and J. J. Brey, Phys. Rev. E **66**, 041308 (2002).
[17] J. J. Brey and A. Prados, Phys. Rev. E **68**, 051302 (2003).
[18] G. C. Barker and A. Mehta, Phys. Rev. A **45**, 3435 (1992).
[19] A. Mehta, G. C. Barker, and J. M. Luck, J. Stat. Mech.: Theory Exp. (2004) P10014.
[20] P. Philippe and D. Bideau, Phys. Rev. E **63**, 051304 (2001).
[21] S. J. Moon, J. B. Swift, and H. L. Swinney, Phys. Rev. E **69**, 031301 (2004).
[22] S. Nasuno, A. Kudrolli, and J. P. Gollub, Phys. Rev. Lett. **79**, 949 (1997).
[23] A. Ferguson and B. Chakraborty, Phys. Rev. E **73**, 011303 (2006).
[24] P. A. Cundall and O. D. L. Strack, Geotechnique **29**, 47 (1979).
[25] P. Ribière, P. Philippe, P. Richard, R. Delannay, and D. Bideau, J. Phys.: Condens. Matter **17**, S2743 (2005).
[26] B. D. Lubachevsky, J. Comput. Phys. **94**, 255 (1991).
[27] O. R. Walton and R. L. Braun, J. Rheol. **30**, 949 (1986).
[28] O. Herbst, M. Huthmann, and A. Zippelius, Granular Matter **2**, 211 (2000).
[29] D. Goldman, M. D. Shattuck, C. Bizon, W. D. McCormick, J. B. Swift, and H. L. Swinney, Phys. Rev. E **57**, 4831 (1998).

[30] E. Falcon, C. Laroche, S. Fauve, and C. Coste, Eur. Phys. J. B **3**, 45 (1998).
[31] S. McNamara and E. Falcon, Phys. Rev. E **71**, 031302 (2005).
[32] S. Miller and S. Luding, Phys. Rev. E **69**, 031305 (2004).
[33] S. F. Foerster, M. Y. Louge, H. Chang, and K. Allia, Phys. Fluids **6**, 1108 (1994).
[34] S. McNamara and W. R. Young, Phys. Rev. E **50**, R28 (1994).
[35] B. Bernu, F. Delyon, and R. Mazighi, Phys. Rev. E **50**, 4551 (1994).
[36] Lj. Budinski-Petković, M. Petković, Z. M. Jakšić, and S. B. Vrhovac, Phys. Rev. E **72**, 046118 (2005).
[37] R. Hilfer, J. Non-Cryst. Solids **305**, 122 (2002).
[38] T. Boutreux and P. G. de Gennes, Physica A **244**, 59 (1997).
[39] F. Ludewig, S. Dorbolo, and N. Vandewalle, Phys. Rev. E **70**, 051304 (2004).
[40] P. Ribière, P. Richard, R. Delannay, and D. Bideau, Phys. Rev. Lett. **95**, 268001 (2005).
[41] G. Marty and O. Dauchot, Phys. Rev. Lett. **94**, 015701 (2005).
[42] E. Ben-Naim, J. B. Knight, E. R. Novak, H. M. Jaeger, and S. R. Nagel, Physica D **123**, 380 (1998).
[43] K. S. Miller and B. Ross, *An Introduction to the Fractional Calculus and Fractional Differential Equation* (Wiley, New York, 1993).
[44] W. Götze and L. Sjögren, Rep. Prog. Phys. **55**, 241 (1992).
[45] M. Tokuyama and Oppenheim, Physica A **216**, 85 (1995).
[46] R. K. Saxena, A. M. Mathai, and H. J. Haubold, Physica A **344**, 657 (2004).
[47] T. Aste, J. Phys.: Condens. Matter **17**, S2361 (2005).
[48] T. Aste, M. Saadatfar, and T. J. Senden, Phys. Rev. E **71**, 061302 (2005).
[49] I. Bratberg, F. Radjai, and A. Hansen, Phys. Rev. E **66**, 031303 (2002).
[50] L. A. Pugnaloni and G. C. Barker, Physica A **337**, 428 (2004).
[51] L. A. Pugnaloni, M. G. Valluzzi, and L. G. Valluzzi, Phys. Rev. E **73**, 051302 (2006).
[52] K. To, P. Y. Lai, and H. K. Pak, Phys. Rev. Lett. **86**, 71 (2001).
[53] F. Aurenhammer, ACM Comput. Surv. **23**, 345 (1991).
[54] P. Richard, P. Philippe, F. Barbe, S. Bourles, X. Thibault, and D. Bideau, Phys. Rev. E **68**, 020301(R) (2003).
[55] T. Aste, Phys. Rev. Lett. **96**, 018002 (2006).
[56] C. Josserand, A. Tkachenko, D. M. Mueth, and H. M. Jaeger, Phys. Rev. Lett. **85**, 3632 (2000).
[57] G. Tarjus and P. Viot, Phys. Rev. E **69**, 011307 (2004).
[58] Lj. Budinski-Petković and S. B. Vrhovac, Eur. Phys. J. E **16**, 89 (2005).